An Investigation on the Current Collection Quality of Railway Pantograph-catenary Systems with Contact Wire Wear Degradations

Song, Yang; Wang, Hongrui; Liu, Zhigang

DOI
10.1109/TIM.2021.3078530

Publication date
2021

Document Version
Final published version

Published in
IEEE Transactions on Instrumentation and Measurement

Citation (APA)
Song, Y., Wang, H., & Liu, Z. (2021). An Investigation on the Current Collection Quality of Railway Pantograph-catenary Systems with Contact Wire Wear Degradations. *IEEE Transactions on Instrumentation and Measurement*, *70*, Article 9003311. https://doi.org/10.1109/TIM.2021.3078530

An Investigation on the Current Collection Quality of Railway Pantograph-Catenary Systems With Contact Wire Wear Degradations

Yang Song, *Member, IEEE*, Hongrui Wang, *Member, IEEE*, and Zhigang Liu, *Senior Member, IEEE*

***Abstract*— In railway pantograph-catenary systems, the contact surfaces undergo wear in long-term operations, directly affecting interaction performance and potentially deteriorating the current collection quality. The effect of contact wire wear (CWW) on the current collection quality should be evaluated to understand the system's health status in operations. This article presents a stochastic analysis of the pantograph–catenary interaction performance with different levels of CWW based on four years of measurement data. The power spectral density (PSD) estimation is carried out on the measured CWW to obtain their frequency representations. The random time histories of CWW are generated based on the PSDs. A nonlinear finite element model of catenary with a lumped-mass pantograph is built. Using the Monte Carlo method, the stochastic analysis of pantograph-catenary contact force is carried out to investigate the distribution and dispersion of assessment indices with different levels of CWW. The results indicate that the CWW mainly affects the maximum and minimum contact forces instead of the contact force standard deviation. The optimal pantograph–catenary interaction performance is observed certain years after CWW is formed, depending on the traffic density of the railway line, which is at the second year in the presented case study. Then, the performance declines with an increase in service time. Also, higher operating speed causes a more significant dispersion in assessment indices representing a lower current collection quality, particularly at the maximum operating speed (70% of the catenary wave propagation speed).**

***Index Terms*— Contact force, contact wire wear (CWW), current collection quality, electrified railway, pantograph–catenary interaction, stochastic analysis.**

I. Introduction

THE overhead contact line, also called catenary constructed along the electrified railway, is responsible for transmitting continuous electric current to the locomotive via pantographs on the car body roof. As shown in Fig. 1, the catenary is the source of power and the pantograph is the power collector. The sliding contact between the registration strip of the pantograph and the contact wire of the catenary transmits electric current through the contact point. The interaction performance directly determines the current collection quality and restricts the maximum operating speed of trains. A stable contact force between the pantograph and the catenary is desired to maintain a reliable pantograph-catenary contact.

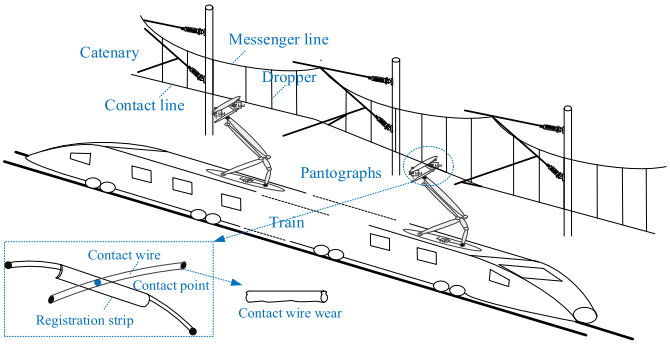

Fig. 1. Schematic of a pantograph-catenary system.

In real-life operation, the pantograph-catenary contact is subjected to internal disturbances from contact-induced vibrations and external disturbances from the environment. Ensuring good interaction performance of pantograph-catenary under harsh operating conditions has been a critical issue for railway operators to avoid train service disruptions, as the pantograph-catenary is widely recognized as the most vulnerable link in railway traction power system without any backups.

A. Problem Description

In long-term operations, the catenary and pantograph's contact surfaces undergo wear, which is the primary source of irregularities that affect the pantograph–catenary interaction. As shown in Fig. 1, the contact wire wear (CWW) can be seen as additional small displacements on the contact point, which contributes a short-wavelength irregularity to the contact wire and directly affects the sliding contact. The evolvement of CWW is a dynamic process, and the severity of the irregularity caused by the CWW develops higher with the increase of service time, which results in an incremental impact on the pantograph–catenary interaction performance.

In the current standard for pantograph–catenary interaction [1], the contact force should be restricted to a specific range, which is normally defined by some time-domain statistical

Manuscript received January 10, 2021; revised April 12, 2021; accepted May 2, 2021. Date of publication May 10, 2021; date of current version May 24, 2021. This work was supported in part by the National Natural Science Foundation of China under Grant U1734202 and Grant 51977182. The Associate Editor coordinating the review process was Dr. Yong Yan. *(Corresponding author: Hongrui Wang.)*

Yang Song is with the Department of Structural Engineering, Norwegian University of Science and Technology, 7491 Trondheim, Norway (e-mail: y.song_ac@hotmail.com).

Hongrui Wang is with the Department of Engineering Structures, Delft University of Technology, 2628 CN Delft, The Netherlands (e-mail: soul_wang0@163.com).

Zhigang Liu is with the School of Electrical Engineering, Southwest Jiaotong University, Chengdu 610031, China (e-mail: liuzg_cd@126.com).

Digital Object Identifier 10.1109/TIM.2021.3078530

indices, such as the standard deviation, maximum, minimum, and mean values. Numerical simulations can be used in the design phase to check the acceptance of the contact force with specific design parameters. However, the simulations are mostly conducted in an ideal condition without real-life disturbances. The CWW, as a primary disturbance in the pantograph–catenary interaction, can definitely affect these assessment indices. Therefore, the pantograph–catenary interaction performance is desired to be re-evaluated with real-life CWW at different stages in the whole service life, which is essential to understand the system's health status after years of operation.

B. Literature Review

In recent decades, the pantograph-catenary dynamics has gained ever-increasing interests from the scientific community, as it is an essential issue for enabling a faster and more reliable operation of electric trains. In the majority of previous studies, numerical models of catenary have been developed based on the methods of the analytical formulation [2], the mode superposition [3], the finite difference [4], and the finite element [5]. The finite element method has been the most preferred method due to the catenary's intrinsic nonlinearity and complex geometry. The pantograph is typically assumed as two or three lumped masses, of which parameters are obtained through experimental testing [6].

Understanding the effects of external disturbances on the pantograph–catenary interaction is crucial for controlling the current collection quality, particularly with speed upgrades. The most common disturbances to the pantograph-catenary are environmental wind loads [7], [8], electromagnetic forces [9], and vehicle-track vibrations [10], which deteriorate the interaction performance and may cause the dewirement of pantographs. A significant consequence of the bad interaction performance is the contact loss between the contact wire and the registration strip, which leads to frequent electric arcing, shortening the system service life [11] and causing power quality issues [12]. This is why various optimization approaches [13] and control strategies [14], [15] are developed to regulate the contact force and ensure stable contact between the pantograph and catenary. With the development of machine learning techniques, data-driven models for pantograph-catenary have been an alternative to evaluating dynamic performance [16].

Apart from external disturbances, the pantograph-catenary internal defects or anomalies are another main source of disturbance that challenges stable and safe operation [17]. The catenary suffers repetitive impacts in its long-term operation, together with potential mounting imprecisions and maintenance inadequacies, which result in the irregularities of the contact wire. An entropy-based detection method also points out that contact wire irregularities have an increasingly negative impact on the contact forces with the increase in service time [18]. Generally, the contact wire irregularities have two sources: one is geometrical distortion and the other is wearing. With the help of measurement data, the geometrical distortion can be appropriately included in the catenary model [19], and its stochastic effect on the contact forces is investigated [20]. Regarding the wear, the existing researches mainly focus on the detection [21], the revelation of generation mechanism [22], and the analysis of evolvement procedures [23] using field or laboratory tests. The deterioration of the current collection quality with the degradation of CWW has not been identified and quantified in the literature. It can be expected that the current collection quality will become worse with the evolvement of CWW. To master the pantograph-catenary system's health status, it is necessary to predict the interaction performance with CWW in different evolvement stages, which is beneficial for designers and operators to evaluate the current collection quality in a whole life cycle.

C. Contribution of This Article

According to the summarized shortcomings in previous researches, this article aims to present a methodology to analyze the current collection quality of pantograph-catenary, including the degradation of CWW. To the best of the authors' knowledge, there are two main challenges in this work. The first one is the acquisition of realistic CWW at different degradation stages. The other one is the characterization of the stochastic nature of CWW in the assessment of current collection quality. For the first challenge, four years of measurement data of CWW collected from a section of the Dutch railway are adopted in this article. These data are used as an input for generating synthetic CWW at different degradation stages and evaluating the pantograph-catenary performance. Regarding the second challenge, the power spectral density (PSD) estimation is carried out on the measured CWW to obtain the frequency characteristics of the given CWW. Adopting the idea to tackle track irregularities [24], the random time history of CWW can be generated according to the PSDs based on an inverse transform. The simulation tool used in this article is a developed nonlinear finite element model of catenary with a lumped-mass pantograph model [25]. This model can capture the high-frequency behavior of pantograph-catenary and has been validated against the measurement data and a worldwide benchmark [26]. In combination with the Monte Carlo method [27], the stochastic analysis of the contact force is carried out with different levels of CWW and operating speeds.

II. Description of Measurement CWW

The measurement data of CWW were collected from a section of a catenary in the Dutch railway network. The measured catenary was operating with regular train traffic on a daily basis during the four years of measurement. The four years of contact wire thickness, with a nominal value of 12 mm, was measured yearly by a specialized inspection train and preprocessed to have a fixed sampling interval of 0.5 m. The preprocessed data used in this study are shown in Fig. 2(a). The CWW can be calculated by removing the nominal value from the measured thickness. The spatial positions of sampling points are recorded simultaneously using a GPS device equipped on-board the measurement vehicle. During the four years of measurement, the measured contact wires have not been replaced or maintained. Therefore, the degradation of CWW can be observed at the same spatial positions.

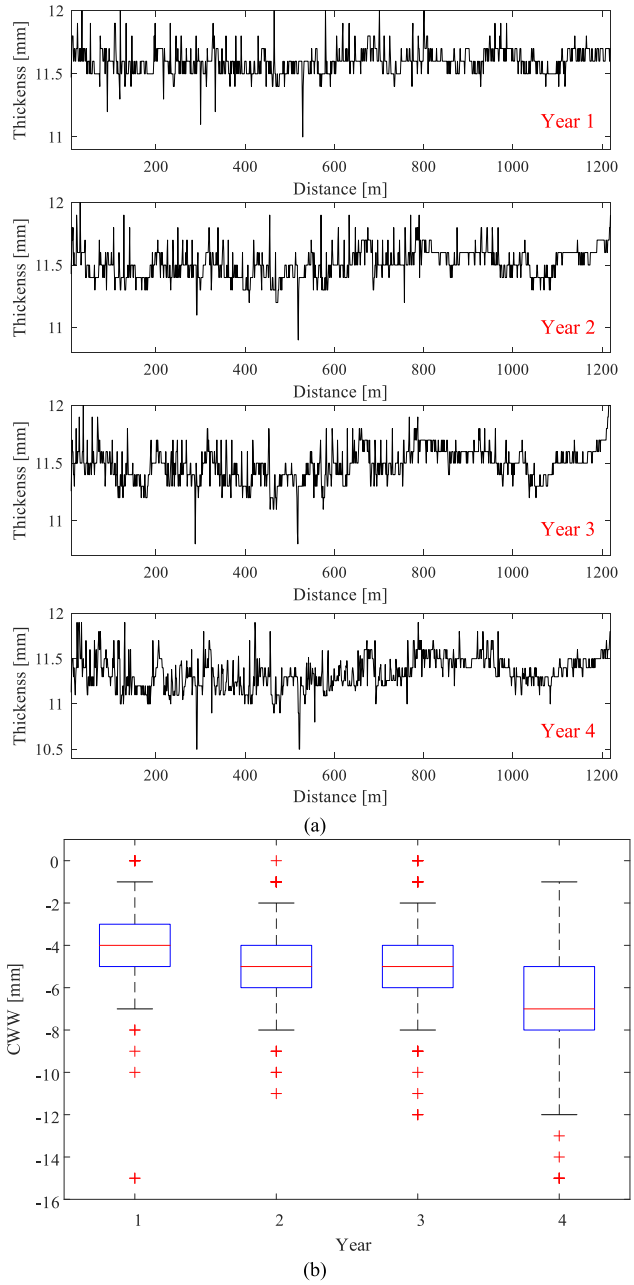

Fig. 2. Four years of CWW measurement. (a) Contact wire thickness measured from year 1 to year 4 (from top to bottom). (b) Boxplot of CWW in 4 years.

Observing the CWW evolution in the four years of operation, the boxplot of CWW is shown in Fig. 2(b). It is seen that the average CWW undergoes a continuous increase by about 0.09-mm per year. The dispersion of CWW shows an incremental trend with the increase in service time. The degradation of CWW has an increasing impact on the contact quality of the pantograph and catenary. Thus, the interaction performance of pantograph and catenary should be evaluated by including the effect of the CWW.

III. Modeling of the Pantograph-Catenary

The schematics of the pantograph-catenary model with CWW are shown in Fig. 3. To characterize the nonlinearity and

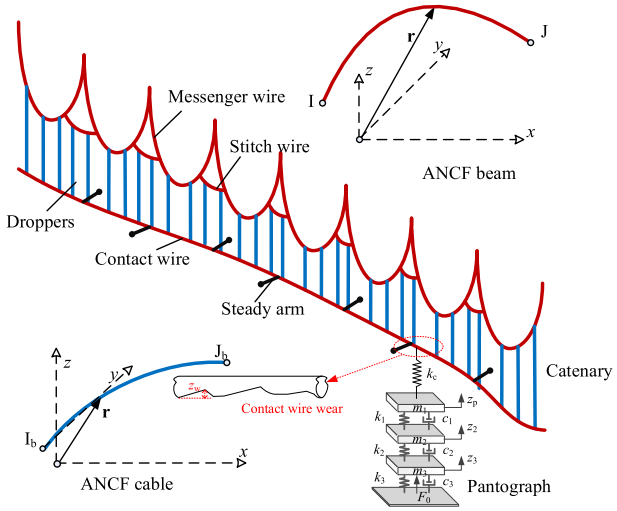

Fig. 3. Schematics of the pantograph-catenary model.

complex initial configuration, the absolute nodal coordinate formulation (ANCF) is used to model the catenary. The pantograph is considered as a lumped-mass model, and the effect of CWW is introduced as an additional vertical displacement of the contact wire. The details of the pantograph-catenary model are described in this section.

A. Modeling of the Catenary

The ANCF is a widely used nonlinear finite element method in different engineering applications [28] to simulate large structural deformations. As shown in Fig. 3, the ANCF beam is utilized to model the contact, messenger, and stitch wires. The ANCF bar is employed to model the dropper and the steady arm. The other accessories, like claws and clamps, are assumed as lumped masses. Considering an ANCF beam element, the nodal degree of freedom (DoF) vector containing the displacements and the gradients can be expressed as

$$\mathbf{e}=\left[x_i \quad y_i \quad z_i \quad \frac{\partial x_i}{\partial \chi} \quad \frac{\partial y_i}{\partial \chi} \quad \frac{\partial z_i}{\partial \chi} \quad x_j \quad y_j \quad z_j \quad \frac{\partial x_j}{\partial \chi} \quad \frac{\partial y_j}{\partial \chi} \quad \frac{\partial z_j}{\partial \chi}\right]^T \tag{1}$$

in which χ is the local longitudinal coordinate in the undeformed configuration from 0 to the element length l_0. The position vector in the deformed configuration $\mathbf{r}$ can be interpolated using the shape function matrix $\mathbf{S}$ as

$$\mathbf{r} = \mathbf{S}\mathbf{e} \tag{2}$$

in which $\mathbf{S}$ is a 3×12 matrix, which is defined using a classic form of shape function for beam element as follows:

$$\mathbf{S} = \begin{bmatrix} S_1 & & & S_2 & & & S_3 & & & S_4 & & \\ & S_1 & & & S_2 & & & S_3 & & & S_4 & \\ & & S_1 & & & S_2 & & & S_3 & & & S_4 \end{bmatrix}$$

$$\begin{aligned} S_1(\xi) &= 1 - 3\xi^2 + 2\xi^3 \\ S_2(\xi) &= l_0(\xi + \xi^3 - 2\xi^2) \\ S_3(\xi) &= 3\xi^2 - 2\xi^3 \\ S_4(\xi) &= l_0(\xi^3 - \xi^2) \end{aligned} \tag{3}$$

in which $\xi = (\chi / l_0)$.

The strain energy of the beam element can be calculated by the summation of the contributions of the axial and bending deformations as

$$U = \frac{1}{2}\int_0^{l_0} (EA\varepsilon_l^2 + EI\kappa^2) d\chi \tag{4}$$

in which E is the elastic modulus, A is the section area, I is the inertial moment of the beam, ε_l is the longitudinal strain, and κ is the curvature. Differentiating the strain energy by the element DoF vector $\mathbf{e}$yields the generalized elastic force vector $\mathbf{Q}$ as follows:

$$\mathbf{Q} = \left(\frac{\partial U}{\partial \mathbf{e}}\right)^{\mathrm{T}} = \mathbf{K}_{\mathrm{e}}\mathbf{e}. \tag{5}$$

According to form (5), the element stiffness matrix $\mathbf{K}_{\mathrm{e}}$ can be defined. It should be noted that $\mathbf{K}_{\mathrm{e}}$ is the secant stiffness matrix relative to the absolute displacements. In numerical simulations, the tangent stiffness matrix $\mathbf{K}_{\mathrm{T}}$ is mainly used to calculate the incremental nodal DoF vector $\Delta\mathbf{e}$. Particularly, in the shape-finding procedure, the tangent stiffness matrix $\mathbf{K}_{\mathrm{L}}$ related to the incremental unstrained length Δl_0 is also required to determine the unstrained length of each element. The corresponding tangent stiffness matrices $\mathbf{K}_{\mathrm{T}}$ and $\mathbf{K}_{\mathrm{L}}$ are derived by

$$\Delta\mathbf{F} = \frac{\partial \mathbf{Q}}{\partial \mathbf{e}}\Delta\mathbf{e} + \frac{\partial \mathbf{Q}}{\partial L_0}\Delta l_0 = \mathbf{K}_{\mathrm{T}}\Delta\mathbf{e} + \mathbf{K}_{\mathrm{L}}\Delta l_0. \tag{6}$$

The tangent stiffness matrices of the ANCF bar element can be similarly obtained. It should be noted that the bar element used to describe the nonlinear behavior of droppers can only withstand tension but not compression. The axial stiffness is set to zero when the dropper works in compression. Assembling the element matrices by the FEM yields the global incremental equilibrium equation for the whole catenary as follows:

$$\Delta\mathbf{F}^{\mathrm{G}} = \mathbf{K}_{\mathrm{T}}^{\mathrm{G}}\Delta\mathbf{U}_{\mathrm{C}} + \mathbf{K}_{\mathrm{L}}^{\mathrm{G}}\Delta\mathbf{L}_0 \tag{7}$$

where $\Delta\mathbf{F}^{\mathrm{G}}$ is the global unbalanced force vector. $\mathbf{K}_{\mathrm{T}}^{\mathrm{G}}$ and $\mathbf{K}_{\mathrm{L}}^{\mathrm{G}}$ are the global stiffness matrices related to the incremental nodal displacement vector $\Delta\mathbf{U}_{\mathrm{C}}$ and the incremental unstrained length vector $\Delta\mathbf{L}_0$, respectively. It should be noted that $[\mathbf{K}_{\mathrm{T}}^{\mathrm{G}} \ \ \mathbf{K}_{\mathrm{L}}^{\mathrm{G}}]$ is not a square matrix, which means that the total number of unknowns in (7) exceeds the total number of equations. Additional constraint conditions must be provided to ensure the unique solutions of (7). Thus, the following additional constraint conditions are defined to suppress the undesired movements according to the design specification.

1) The vertical positions of the dropper point in the contact wire are restricted to describe the reserved presag.
2) The longitudinal direction of each node is restricted to suppress the longitudinal movement.
3) The tensions are applied to each stitch wire.
4) The tensions are applied to the endpoints of messenger and contact wires.

With the help of the above extra constraints, the Newton–Raphson iteration is utilized to solve the initial configuration of the catenary. Introducing a consistent mass matrix and a Rayleigh damping, the equation of motion for the catenary is written as

$$\mathbf{M}_{\mathrm{C}}^{\mathrm{G}}\ddot{\mathbf{U}}_{\mathrm{C}}(t) + \mathbf{C}_{\mathrm{C}}^{\mathrm{G}}\dot{\mathbf{U}}_{\mathrm{C}}(t) + \mathbf{K}_{\mathrm{C}}^{\mathrm{G}}(t)\mathbf{U}_{\mathrm{C}}(t) = \mathbf{F}_{\mathrm{C}}^{\mathrm{G}}(t) \tag{8}$$

in which $\mathbf{M}_{\mathrm{C}}^{\mathrm{G}}$, $\mathbf{C}_{\mathrm{C}}^{\mathrm{G}}$, and $\mathbf{K}_{\mathrm{C}}^{\mathrm{G}}(t)$ are the mass, damping, and stiffness matrices, respectively. $\mathbf{F}_{\mathrm{C}}^{\mathrm{G}}(t)$ is the external force vector which contains the contact force and gravity.

B. Modeling of the Pantograph and Contact

The lumped-mass model of the pantograph is an efficient reproduction of the first several critical modes of a real one. The interaction between the pantograph head and the contact wire is modeled by a penalty function method based on the relative penetration δ on the contact surface. The contact force f_c is calculated by the product of the contact stiffness k_{s} and the penetration δ as follows:

$$f_c = \begin{cases} k_{\mathrm{s}}\delta, & \text{if } \delta > 0 \\ 0, & \text{if } \delta \le 0. \end{cases} \tag{9}$$

It should be noted that the penetration δ can be evaluated by

$$\delta = z_{\mathrm{p}} - z_{\mathrm{c}} - z_{\mathrm{w}} \tag{10}$$

in which z_{p}, z_{c}, and z_{w} are the vertical displacements of the pantograph head, the contact wire at the contact point, and the CWW, respectively. By including (9), the equation of motion for the pantograph-catenary system including the effect of wear is written as

$$\mathbf{M}^{\mathrm{G}}\ddot{\mathbf{U}}(t) + \mathbf{C}^{\mathrm{G}}\dot{\mathbf{U}}(t) + \mathbf{K}^{\mathrm{G}}(t)\mathbf{U}(t) = \mathbf{F}^{\mathrm{G}}(t) \tag{11}$$

in which, $\mathbf{M}^{\mathrm{G}}$, $\mathbf{C}^{\mathrm{G}}$, and $\mathbf{K}^{\mathrm{G}}(t)$ are the mass, damping, and stiffness matrices for the whole system, respectively. $\mathbf{F}^{\mathrm{G}}(t)$ is the external force vector. A Newmark integration scheme is adopted to solve (11). The stiffness matrix $\mathbf{K}^{\mathrm{G}}(t)$ is updated in each time step to fully describe the geometrical nonlinearity of wears and the slackness of droppers.

IV. Prediction of Stochastic Performance

The stochastic nature of CWW leads to indeterministic behaviors of pantograph–catenary interaction. The traditional deterministic analysis may not be allowed to evaluate the performance of pantograph-catenary with stochastic perturbations. In this work, the frequency representation of the measured CWW is obtained using PSD estimation. Then, a reasonable number of CWW time-histories are generated from the PSD using the inverse Fourier transform. By introducing the CWW into the physical numerical model, the distribution and dispersion of the assessment indices with different CWW levels can be evaluated based on the Monte Carlo method [29]. Generally, the concept of the prediction procedure relies on a model-based method, as shown in Fig. 4. The traditional pantograph-catenary model only uses the design parameters to predict the ideal results, which can only be used in the design phase to check the acceptance of the design. The realistic behavior cannot be predicted as practical disturbances are not included. This article includes the most common perturbance, the CWW, in the pantograph-catenary model

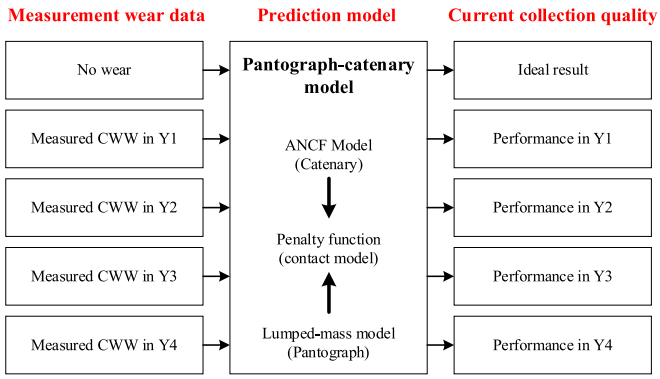

Fig. 4. Model-based predictions of current collection quality.

to predict the current collection quality in the four years of service. The current deterministic analysis, which relies on the results from a single simulation, cannot describe the dispersion of the response caused by stochastic perturbations. Based on the Monte Carlo method, a considerable amount of simulations can be carried out to fully describe the stochastic behavior. Considering the computational effort, 1000 samples are generated and adopted to describe the effect of stochastic CWW for each case. The flowchart to predict the stochastic performance of pantograph-catenary under stochastic CWW is shown in Fig. 5.

A. PSD Estimation of CWW

The PSD estimation is carried out to obtain the frequency representation of the measured CWW. The traditional PSD estimation is non-parametric and normally based on the results of Fourier transform using the periodogram method and the enhanced periodogram methods. To overcome the spectral leakage problem, the autoregressive (AR) model is developed. For a discrete process with N data samples $\{x(n);\, n = 1.2, \ldots, N\}$, the basic form of the AR model can be written as

$$x(n) = \sum_{k=1}^{p} a_k x(n-k) + e_n \tag{12}$$

where p is the order of the AR model, a_k is the AR coefficient, and e_n is a white noise process with zero mean and variance σ_e^2. The PSD estimated by the AR model is expressed by

$$S(\omega) = \frac{\sigma_e^2}{\left|1 - \sum_{k=1}^{p} a_k e^{-i\omega k}\right|^2} \tag{13}$$

in which σ_e^2 and a_k can be estimated by solving the Yule–Walker equations.

B. CWW Time-Histories From PSD

The time-histories of CWW with the same frequency characteristics of the measurement data are obtained from the PSD by the inverse Fourier transform. The frequency spectrum $P(m)$ is obtained by discrete sampling from the standard spectral density $S(f)$. The real and imaginary parts of $P(m)$ have both even and odd symmetries with respect to $N/2$. Hence, the frequency spectrum $P(m)$ is determined by

$$P(m) = |P(m)|(\cos\phi_m + i\sin\phi_m) \quad (m = 0, 1, \ldots, N/2) \tag{14}$$

where ϕ_m is the phase angle and obeys the uniform distribution of $0 \sim 2\pi$. Then, the time-history is calculated using the inverse Fourier transform as follows:

$$y(n) = \frac{1}{N}\sum_{m=0}^{N-1} P(m)\exp\left[\frac{i2\pi mn}{N}\right] \quad (n = 0, 1, \ldots, N-1). \tag{15}$$

Taking the CWW measured in year 4 (Y4) as an example to validate the above-mentioned method, the comparison of original and 1000 generated PSDs is shown in Fig. 6. The excellent consistency of generated PSDs against the original one shows the validity of the presented method to generate time-histories of CWW, which can be used in the subsequent stochastic analysis.

C. Assessment Index

The technical criteria of the pantograph–catenary interaction [30] specify that the contact force with 20 Hz cut-off frequency is the most critical quantity as it directly describes the current collection quality. The mean contact force F_m is tuned according to the specification of EN 50367 for each case as

$$F_m = 0.00097v^2 + 70 \tag{16}$$

where v is the train speed. Usually, the standard deviation σ is used to evaluate the fluctuations of the contact force. The maximum contact force is adopted to check the safety acceptance. Remarkably, the minimum contact force should be restricted as an inadequate contact force may increase the occurrence of contact loss, leading to arcing and the interruption of electric transmission.

To facilitate the analysis of the stochastic behaviors with random CWW, the boxplot is utilized to present the assessment indices. The boxplot is a standardized way to display the distribution of data based on a summary of five numbers: the minimal value $Q_{\min}$, the first quartile Q_1, the median Q_2, the third quartile Q_3, and the maximal value $Q_{\max}$. Usually, the maximal and minimal can be calculated, respectively, by the following two equations:

$$Q_{\max} = Q_3 + 1.5 \times IQR \tag{17a}$$

$$Q_{\min} = Q_1 - 1.5 \times IQR \tag{17b}$$

in which IQR is the range from the 25th to 75th percentile. With the help of a boxplot, the dispersion of each assessment index can be directly analyzed.

A continuous catenary structure modeled by the parameters in [23] traversed by double pantographs is taken as the analysis object. The catenary geometry is shown in Fig. 7. To eliminate the simulation's boundary effect, the contact forces from 360 to 780 m for both pantographs are adopted in the subsequent analysis. The pantograph is modeled based on a WBL85-type

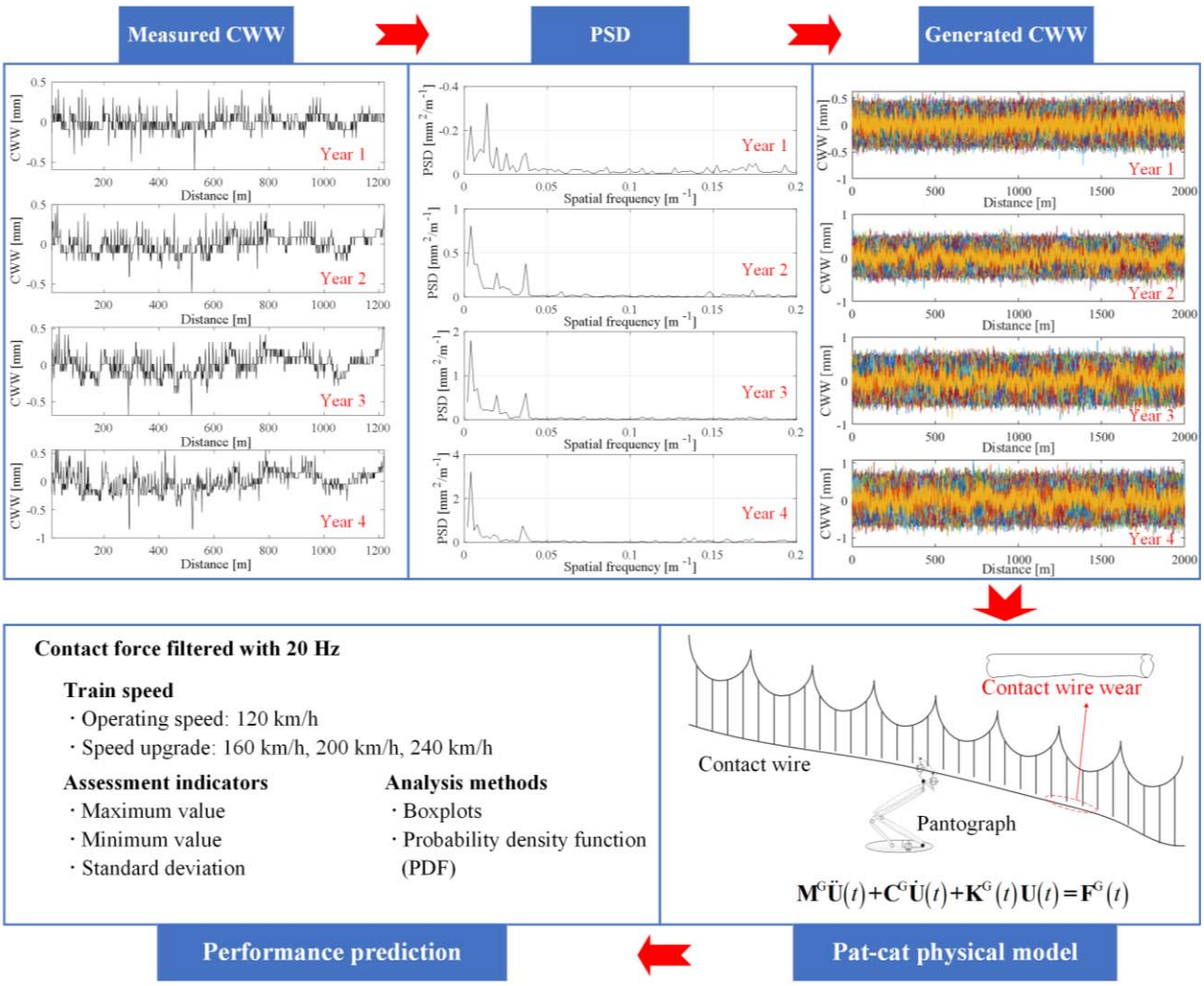

Fig. 5. Prediction procedure of current collection quality with measured CWW.

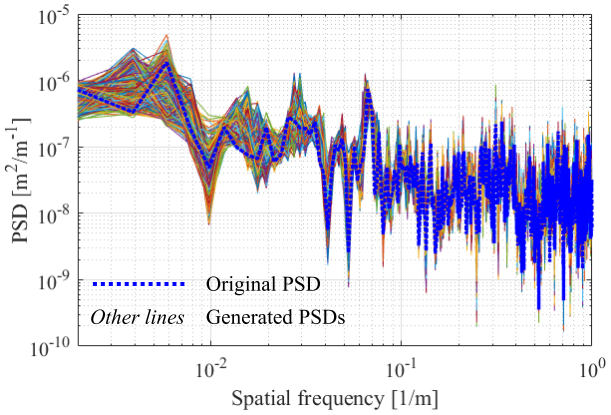

Fig. 6. Comparison of generated PSDs and original PSD.

pantograph, which is widely used in Nordic countries. The interval for the double pantographs is 200 m.

V. Analysis Under Operating Speed and Speed Upgrade

In this section, the operating speed (120 km/h) is used in the simulation to analyze the pantograph–catenary system's interaction performance with different levels of CWW. The overview of the stochastic analysis is shown in Fig. 8. The boxplot of contact force statistics (including the standard deviation, the maximum value, and the minimum value) is adopted to analyze the dispersion of responses. Speed upgrades (160, 200, and 240 km/h) are adopted in the simulations to investigate the contact force dispersions. The PDF of the minimum contact force is analyzed to predict the reliability of the system in different service years.

A. CWW Effects With Operating Speed

In this section, the contact force is analyzed with CWW for the four service years at an operating speed of 120 km/h. The boxplots of contact force standard deviation for the leading and trailing pantographs are shown in Fig. 9(a) and (b), respectively. The result without CWW is presented using a purple dash-dotted line. It is seen that the CWW leads to a slight dispersion of the standard deviation for both pantographs. The lowest standard deviation appears in Y2. This can be explained by the theory of the bathtub curve [31]. Normally, the best performance of a mechanical system can be achieved after the initial period of operation. For the analyzed case, the

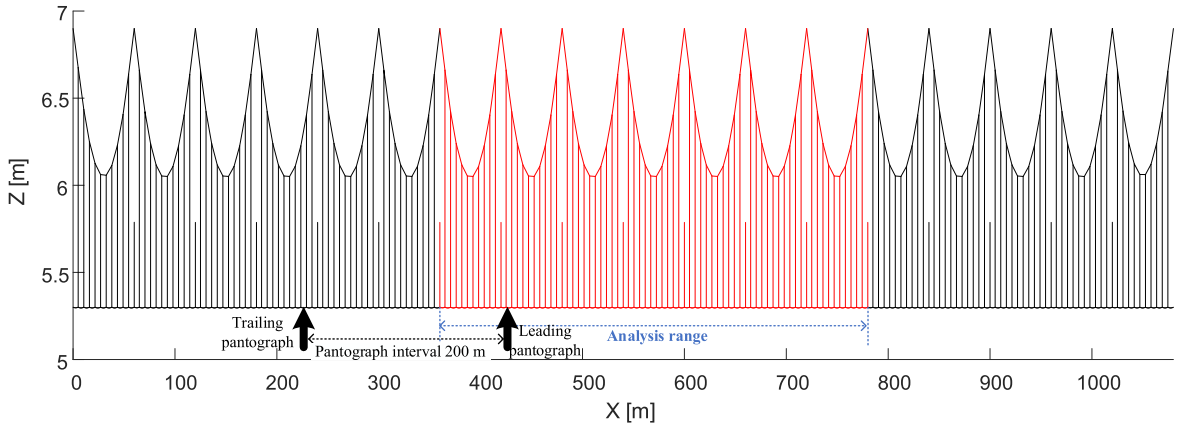

Fig. 7. Catenary geometry and analysis range.

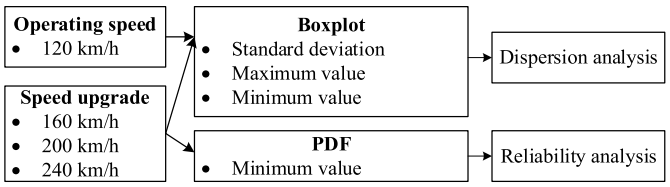

Fig. 8. Overview of the stochastic analysis.

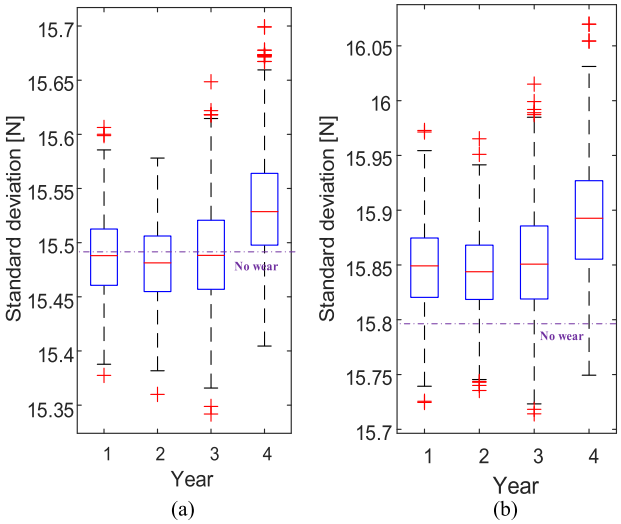

Fig. 9. Boxplots of the standard deviation for the (a) leading and (b) trailing pantographs at 120 km/h.

pantograph-catenary reaches the best performance after two years of operation. After Y2, the performance becomes worse with the increase in CWW.

Fig. 10(a) and (b) shows the boxplots of maximum contact force for the leading and trailing pantographs, respectively. Unlike the standard deviation, the dispersion of the maximum contact force caused by the CWW is much more notable. The dispersion becomes smaller from Y1 to Y2, while it undergoes a sharp increase from Y2 to Y4. The difference between the maximum and the minimum values in the 1000 cases is over 4 N for all cases. A similar trend can be seen in Fig. 11(a) and (b), which presents the boxplots of minimum

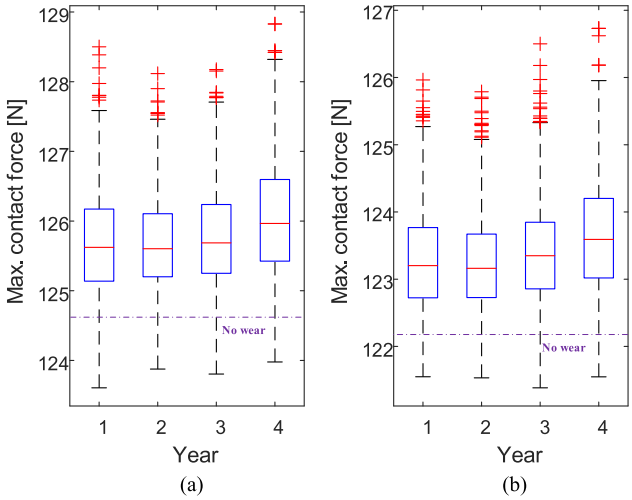

Fig. 10. Boxplots of maximum contact force for the (a) leading and (b) trailing pantographs at 120 km/h.

contact force for the leading and trailing pantographs, respectively. The minimum contact force has a smaller dispersion in Y2 than Y1, which also increases from Y2 to Y4.

B. CWW Effects With Speed Upgrades

According to EN 50119 [32], the maximum speed for a catenary can be calculated by 70% of the wave propagation speed, which is about 240 km/h for the analysis object. In this section, the train speeds vary from 160 to 240 km/h with a 40-km/h interval to carry out the numerical simulation to analyze the contact forces simulated under different levels of CWW. The analysis results in the previous subsection A indicate that the CWW does not have an evident effect on the contact force standard deviation. In this section, only the maximum and minimum contact forces are analyzed.

At 160 km/h, the boxplots of maximum and minimum contact force are shown in Figs. 12 and 13, respectively. Similar to the results at 120 km/h, the performance reaches the best level after two years of operation and becomes worse from Y2 to Y4. The dispersion caused by the CWW is more significant than the results evaluated at 120 km/h.

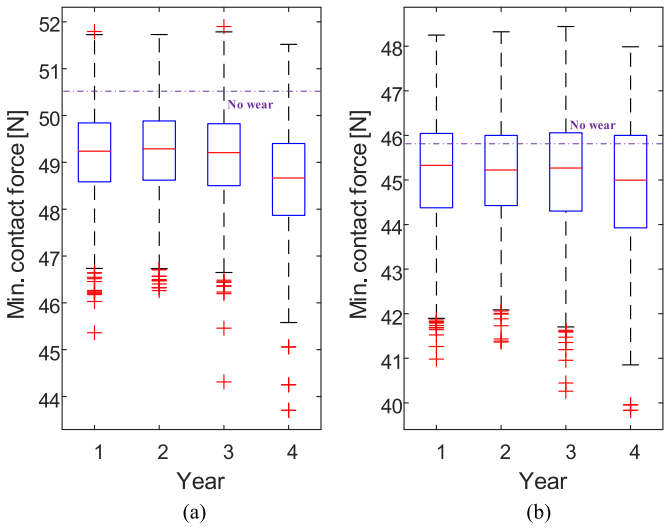

Fig. 11. Boxplots of minimum contact force for the (a) leading and (b) trailing pantographs at 120 km/h.

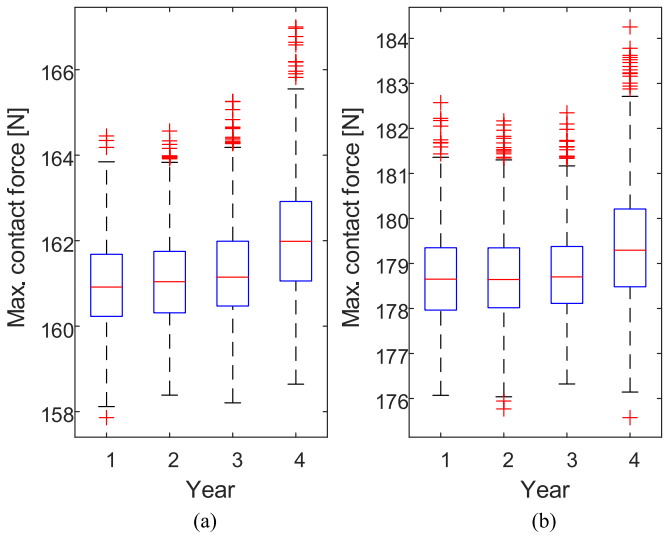

Fig. 12. Boxplots of maximum contact force for the (a) leading and (b) trailing pantographs at 160 km/h.

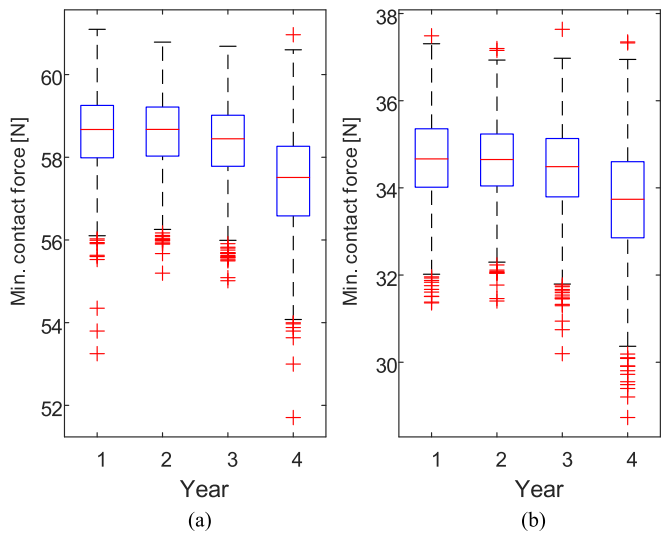

Fig. 13. Boxplots of minimum contact force for the (a) leading and (b) trailing pantographs at 160 km/h.

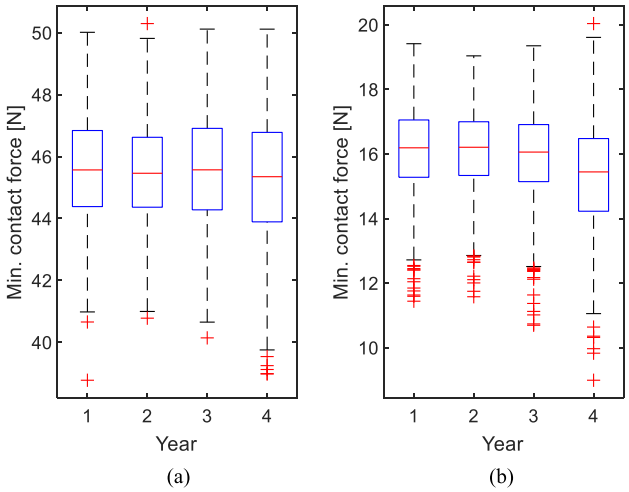

Fig. 14. Boxplots of minimum contact force for the (a) leading and (b) trailing pantographs at 200 km/h.

At 200 km/h, the maximum contact force follows a similar trend as at lower speeds, which is not presented here for conciseness. The boxplots of minimum contact force for the leading and trailing pantographs are shown in Fig. 14(a) and (b), respectively. Besides the larger dispersion caused by the CWW, it is also seen that some minimum contact forces of the trailing pantograph in Y4 are lower than the safety threshold 10 N [1], which may induce long-distance arcing and reduce the life expectancy of the pantograph-catenary. Based on the 1000 simulation results, the histogram of the trailing pantograph's minimum contact force with the Y4 CWW is shown in Fig. 15(a). It is seen that three minimum contact forces are lower than the safety threshold. Based on the normal distribution assumption, the PDF of the minimum contact force of the trailing pantograph is shown in Fig. 15(b). Considering a 99.73% confidence level, the lower bound is 10.54 N, which is slightly higher than the safety threshold. According to the cumulative distribution function, the probability that the minimum contact force is smaller than 10 N in Y4 is 0.042%, which is smaller than the arcing rate threshold of 0.1% specified in EN 50119 [32]. Therefore, it is assumed that the system can still operate normally in Y4 at 200 km/h.

At 240 km/h, the boxplots of minimum contact force for leading and trailing pantographs are shown in Fig. 16(a) and (b), respectively. More minimum contact forces of the trailing pantograph smaller than the safety threshold can be observed in Y3 and Y4. The corresponding histograms are shown in Fig. 17(a). In Y3, only one outlier in 1000 simulations can be observed. However, in Y4 there are 14 outliers. The PDFs of the minimum contact force of the trailing pantograph in Y3 and Y4 are shown in Fig. 17(b). Considering a 99.73% confidence level, the lower bounds for Y3 and Y4 are 9.75 and 8.77 N, respectively, which are lower than the safety threshold. The probabilities that the minimum contact force is smaller than 10 N are 0.76% and

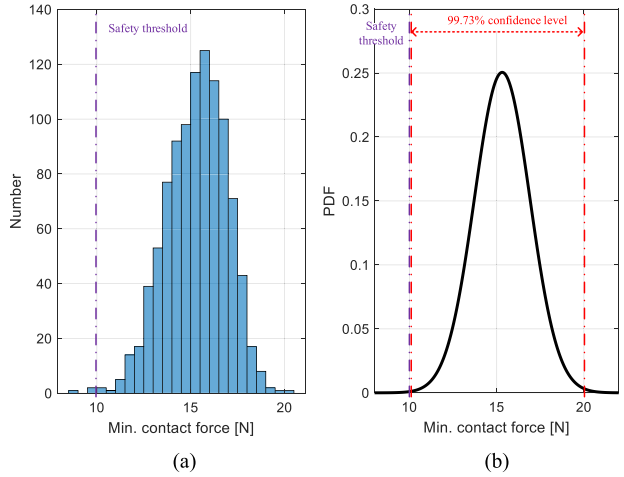

Fig. 15. (a) Histogram and (b) PDF of minimum contact force for the trailing pantograph at 200 km/h.

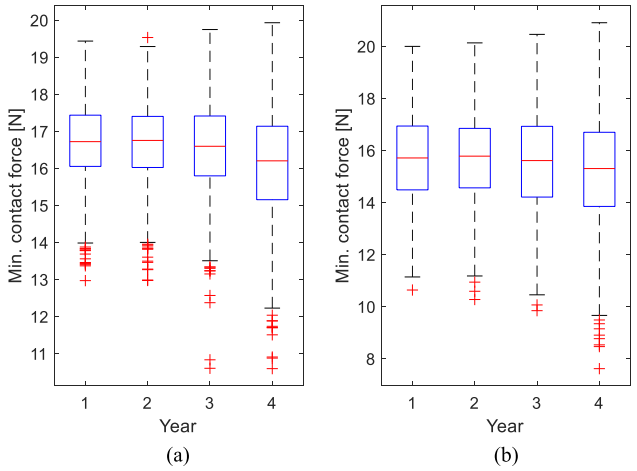

Fig. 16. Boxplots of minimum contact force for the (a) leading and (b) trailing pantographs at 240 km/h.

0.2% in Y3 and Y4, respectively, which both do not satisfy the arcing rate threshold of 0.1% specified in EN 50119 [32]. Therefore, frequent arcing and sparking are expected in Y3 and Y4 if the train operates at 240 km/h. Therefore, a speed upgrade to 240 km/h in such a case is not advised.

C. Discussion

The above analysis presents the performance prediction of the current collection quality with the evolvement of CWW for the four service years. Generally, two main phenomena can be observed from the prediction results. The first one is that the best current collection quality can be achieved after two years of operation. Afterward, the performance declines in the subsequent years. The second one is when the train operates at the maximum possible speed (70% of the catenary wave propagation speed), the minimum contact force does not satisfy the requirement of the standard after Y2.

The first phenomenon can be explained by the classic bathtub curve. The best performance of a mechanical system can be achieved after certain years of operation. The second phenomenon indicates the necessity of probabilistic analysis.

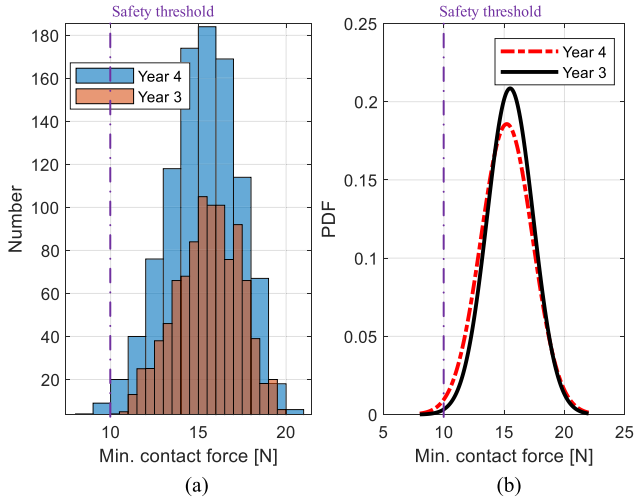

Fig. 17. (a) Histogram and (b) PDF of minimum contact force for the trailing pantograph at 240 km/h.

Due to the stochastic nature of CWW, the system performance has some probability of exceeding the safety threshold. It is recommended that stochastic perturbations should be included in the assessment criteria to improve the current standard.

One of the significant shortfalls in the present analysis is that only four years of CWW data are acquired, so only four years of current collection quality can be predicted. More measurement data are required to predict longer term performances. Measuring the CWW more than once per year can also improve the accuracy for predicting the stochastic behaviors of a catenary in a short time span. Furthermore, this article only presents predictions of the contact forces by including measured CWW in the physical model. In reality, the contact forces can also deteriorate CWW, as indicated in [33]. In the future, the wear model of catenary can be included to make a prediction considering the mutual effects between CWW and contact forces.

VI. Conclusion

This article presents a stochastic analysis of the current collection quality of railway pantograph-catenary with different levels of CWW. Four years of CWW data measured from a section of the Dutch railway are adopted. A pantograph-catenary model considering the effects of CWW is constructed based on real-life parameters. The frequency representation of the measured CWW is obtained to generate 1000 samples of CWW time-histories based on the Monte Carlo method. The distribution and dispersion of the assessment indices of pantograph-catenary contact force with different levels of CWW are evaluated. The main findings of this study can be summarized as follows:

1) The CWW mainly affects the local behavior of the pantograph–catenary interaction (namely the maximum and minimum contact forces) instead of the global behavior (namely the contact force standard deviation).
2) The pantograph–catenary interaction reaches the best performance certain years after installation, which

depends on the traffic density operating on the catenary in the railway line. For the given case of analysis, the pantograph-catenary performance is optimal under the CWW measured in the second year. Afterward, the performance declines in the subsequent years.

3) When the CWW is considered, the upgrade of train speed causes a larger dispersion of assessment indices. When the train operates at the maximum possible speed (70% of the catenary wave propagation speed), the minimum contact force does not satisfy the standard after Y2. Frequent arcing and sparking are expected in practice, which advises against the speed upgrade.

In future studies, CWW data collected for a period longer than four years and measured more than once a year may enable more significant findings on the long-term and short-term behaviors of pantograph–catenary interaction. Also, the evolvement of CWW and pantograph–catenary interaction can be investigated and predicted in a longer timeframe with a higher time resolution.

REFERENCES

[1] European Committee for Electrotechnical Standardization, *Railway Applications–Current Collection Systems–Technical Criteria for the Interaction Between Pantograph and Overhead Line*, document EN 50367, European Standards (EN), Brussels, Belgium, 2012.

[2] Y. Song, Z. Liu, F. Duan, Z. Xu, and X. Lu, "Wave propagation analysis in high-speed railway catenary system subjected to a moving pantograph," *Appl. Math. Model.*, vol. 59, pp. 20–38, Jul. 2018.

[3] G. Mei, W. Zhang, H. Zhao, and L. Zhang, "A hybrid method to simulate the interaction of pantograph and catenary on overlap span," *Vehicle Syst. Dyn.*, vol. 44, no. sup1, pp. 571–580, Jan. 2006.

[4] L. Finner, G. Poetsch, B. Sarnes, and M. Kolbe, "Program for catenary–pantograph analysis, PrOSA statement of methods and validation according EN 50318," *Vehicle Syst. Dyn.*, vol. 53, no. 3, pp. 305–313, 2015.

[5] Y. H. Cho, "Numerical simulation of the dynamic responses of railway overhead contact lines to a moving pantograph, considering a nonlinear dropper," *J. Sound Vib.*, vol. 315, no. 3, pp. 433–454, Aug. 2008.

[6] S. Pil Jung, Y. Guk Kim, J. Sung Paik, and T. Won Park, "Estimation of dynamic contact force between a pantograph and catenary using the finite element method," *J. Comput. Nonlinear Dyn.*, vol. 7, no. 4, Oct. 2012, Art. no. 041006.

[7] Y. Song, Z. Liu, H. Wang, J. Zhang, X. Lu, and F. Duan, "Analysis of the galloping behaviour of an electrified railway overhead contact line using the non-linear finite element method," *Proc. Inst. Mech. Eng., F, J. Rail Rapid Transit*, vol. 232, no. 10, pp. 2339–2352, Nov. 2018.

[8] M. Zhang, F. Xu, and Y. Han, "Assessment of wind-induced nonlinear post-critical performance of bridge decks," *J. Wind Eng. Ind. Aerodyn.*, vol. 203, Aug. 2020, Art. no. 104251.

[9] S. Midya, D. Bormann, Z. Mazloom, T. Schutte, and R. Thottappillil, "Conducted and radiated emission from pantograph arcing in AC traction system," in *Proc. IEEE Power Energy Soc. Gen. Meeting*, Jul. 2009, pp. 1–8.

[10] Y. Song, Z. Wang, Z. Liu, and R. Wang, "A spatial coupling model to study dynamic performance of pantograph-catenary with vehicle-track excitation," *Mech. Syst. Signal Process.*, vol. 151, Apr. 2021, Art. no. 107336.

[11] G. Bucca, A. Collina, R. Manigrasso, F. Mapelli, and D. Tarsitano, "Analysis of electrical interferences related to the current collection quality in pantograph–catenary interaction," *Proc. Inst. Mech. Eng., F, J. Rail Rapid Transit*, vol. 225, no. 5, pp. 483–499, 2011.

[12] Y. Cheng, Z. Liu, and K. Huang, "Transient analysis of electric arc burning at insulated rail joints in high-speed railway stations based on state-space modeling," *IEEE Trans. Transp. Electrific.*, vol. 3, no. 3, pp. 750–761, Sep. 2017.

[13] J. Zhang, W. Liu, and Z. Zhang, "Sensitivity analysis and research on optimisation methods of design parameters of high-speed railway catenary," *IET Elect. Syst. Transp.*, vol. 9, no. 3, pp. 150–156, Sep. 2019.

[14] Y. Song, H. Ouyang, Z. Liu, G. Mei, H. Wang, and X. Lu, "Active control of contact force for high-speed railway pantograph-catenary based on multi-body pantograph model," *Mechanism Mach. Theory*, vol. 115, pp. 35–59, Sep. 2017.

[15] X. Lu, Z. Liu, J. Zhang, H. Wang, Y. Song, and F. Duan, "Prior-information-based finite-frequency H_∞ control for active double pantograph in high-speed railway," *IEEE Trans. Veh. Technol.*, vol. 66, no. 10, pp. 8723–8733, Oct. 2017.

[16] H. Wang, A. Nunez, Z. Liu, D. Zhang, and R. Dollevoet, "A Bayesian network approach for condition monitoring of high-speed railway catenaries," *IEEE Trans. Intell. Transp. Syst.*, vol. 21, no. 10, pp. 4037–4051, Oct. 2020.

[17] J. Chen, Z. Liu, H. Wang, A. Nunez, and Z. Han, "Automatic defect detection of fasteners on the catenary support device using deep convolutional neural network," *IEEE Trans. Instrum. Meas.*, vol. 67, no. 2, pp. 257–269, 2017.

[18] H. Wang, Z. Liu, A. Núñez, and R. Dollevoet, "Entropy-based local irregularity detection for high-speed railway catenaries with frequent inspections," *IEEE Trans. Instrum. Meas.*, vol. 68, no. 10, pp. 3536–3547, Oct. 2019.

[19] Y. Song, P. Antunes, J. Pombo, and Z. Liu, "A methodology to study high-speed pantograph-catenary interaction with realistic contact wire irregularities," *Mechanism Mach. Theory*, vol. 152, Oct. 2020, Art. no. 103940.

[20] Y. Song, Z. Z. Liu, A. Ronnquist, P. Navik, and Z. Z. Liu, "Contact wire irregularity stochastics and effect on high-speed railway pantograph–catenary interactions," *IEEE Trans. Instrum. Meas.*, vol. 69, no. 10, pp. 8196–8206, Oct. 2020.

[21] S. Judek and L. Jarzebowicz, "Algorithm for automatic wear estimation of railway contact strips based on 3D scanning results," in *Proc. Int. Conf. Expo. Electr. Power Eng. (EPE)*, Oct. 2014, pp. 724–729.

[22] A. Collina, S. Melzi, and A. Facchinetti, "On the prediction of wear of contact wire in OHE lines: A proposed model," *Vehicle Syst. Dyn.*, vol. 37, no. sup1, pp. 579–592, Jan. 2002.

[23] H. Wang, A. Núñez, Z. Liu, Y. Song, F. Duan, and R. Dollevoet, "Analysis of the evolvement of contact wire wear irregularity in railway catenary based on historical data," *Vehicle Syst. Dyn.*, vol. 56, no. 8, pp. 1207–1232, Aug. 2018.

[24] W. Zhai and W. Zhai, *Vehicle-Track Coupled Dynamics Models*, 4th ed. Beijing, China Science Press, 2020.

[25] Y. Song, A. Ronnquist, and P. Navik, "Assessment of the high-frequency response in railway pantograph-catenary interaction based on numerical simulation," *IEEE Trans. Veh. Technol.*, vol. 69, no. 10, pp. 10596–10605, Oct. 2020.

[26] S. Bruni *et al.*, "The results of the pantograph–catenary interaction benchmark," *Vehicle Syst. Dyn.*, vol. 53, no. 3, pp. 412–435, Mar. 2015.

[27] Y. I. Jenie, E. J. Van Kampen, J. Ellerbroek, and J. M. Hoekstra, "Safety assessment of a UAV CD&R system in high density airspace using Monte Carlo simulations," *IEEE Trans. Intell. Transp. Syst.*, vol. 19, no. 8, pp. 2686–2695, Aug. 2018.

[28] B. Zemljarič and V. Ažbe, "Analytically derived matrix end-form elastic-forces equations for a low-order cable element using the absolute nodal coordinate formulation," *J. Sound Vib.*, vol. 446, pp. 263–272, Apr. 2019.

[29] Z. Wang, Y. Song, Z. Yin, R. Wang, and W. Zhang, "Random response analysis of axle-box bearing of a high-speed train excited by crosswinds and track irregularities," *IEEE Trans. Veh. Technol.*, vol. 68, no. 11, pp. 10607–10617, Nov. 2019.

[30] European Committee for Electrotechnical Standardization, *Railway Applications–Current Collection Systems–Technical Criteria for the Interaction Between Pantograph and Overhead Line*, European Standards (EN), Brussels, Belgium, Standard EN 50367, 2016.

[31] G. Klutke, P. C. Kiessler, and M. A. Wortman, "A critical look at the bathtub curve," *IEEE Trans. Rel.*, vol. 52, no. 1, pp. 125–129, Mar. 2003.

[32] European Committee for Electrotechnical Standardization, *Railway Applications–Fixed Installations–Electric Traction Overhead Contact Lines*, European Standards (EN), Brussels, Belgium, Standard EN 50119, 2013.

[33] S. Daocharoenporn, M. Mongkolwongrojn, S. Kulkarni, and A. A. Shabana, "Prediction of the pantograph/catenary wear using nonlinear multibody system dynamic algorithms," *J. Tribol.*, vol. 141, no. 5, May 2019, Art. no. 051603.

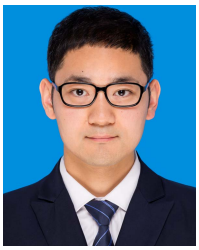

Yang Song (Member, IEEE) received the Ph.D. degree from Southwest Jiaotong University, Chengdu, Sichuan, China, in 2018.

From October 2018 to September 2019, he has worked as a Research Fellow with the Institute of Railway Research, University of Huddersfield, Huddersfield, U.K. He is currently a Postdoctoral Researcher with the Department of Structural Engineering, Norwegian University of Science and Technology, Trondheim, Norway. His research interests include the assessment of railway pantograph–OCL interactions and the wind-induced vibration of long-span structures in railway transportation.

Hongrui Wang (Member, IEEE) received the Ph.D. degree from the Section of Railway Engineering, Delft University of Technology, Delft, The Netherlands, in 2019.

He was a Postdoctoral Researcher with the Delft University of Technology until November 2020, where he is currently an Assistant Professor with the Department of Engineering Structures. His research interests include signal processing, artificial intelligence, and their applications in the structural health monitoring and digital modeling of railway infrastructures.

Dr. Wang is an Associate Editor of the IEEE TRANSACTIONS ON INSTRUMENTATION AND MEASUREMENT journal.

Zhigang Liu (Senior Member, IEEE) received the Ph.D. degree in power systems and their automation from Southwest Jiaotong University, Chengdu, Sichuan, China, in 2003.

He is currently a Full Professor with the School of Electrical Engineering, Southwest Jiaotong University. He has written three books and published more than 150 peer-reviewed journal articles and conference papers. His research interests include the electrical relationship of EMUs and traction, and detection and assessment of pantograph-catenary in high-speed railway.

Dr. Liu was elected as a fellow of the Institution of Engineering and Technology (IET) in 2017. He received the IEEE TRANSACTIONS ON INSTRUMENTATION AND MEASUREMENTS Outstanding Associate Editor in 2019 and 2020 and an Outstanding Reviewer of IEEE TRANSACTIONS ON INSTRUMENTATION AND MEASUREMENT in 2018. He is an Associate Editor of IEEE TRANSACTIONS ON NEURAL NETWORKS AND LEARNING SYSTEMS, IEEE TRANSACTIONS ON VEHICULAR TECHNOLOGY, IEEE TRANSACTIONS ON INSTRUMENTATION AND MEASUREMENT, and IEEE ACCESS.